Velocity and attitude estimation of a small unmanned aircraft with micro Pitot tube and Inertial Measurement Unit (IMU)

Conference Paper · June 2020

DOI: 10.1109/MetroAeroSpace48742.2020.9160298

4 authors:

Gennaro Ariante
Parthenope University of Naples
6 PUBLICATIONS **10** CITATIONS
SEE PROFILE

Umberto Papa
Parthenope University of Naples
29 PUBLICATIONS **147** CITATIONS
SEE PROFILE

Salvatore Ponte
Università degli Studi della Campania "Luigi Vanvitelli
9 PUBLICATIONS **27** CITATIONS
SEE PROFILE

Giuseppe Del Core
Parthenope University of Naples
38 PUBLICATIONS **246** CITATIONS
SEE PROFILE

Velocity and attitude estimation of a small unmanned aircraft with micro Pitot tube and Inertial Measurement Unit (IMU)

Gennaro Ariante
Department of Science and Technology
Parthenope University of Naples
Naples, Italy
gennaro.ariante@uniparthenope.it

Umberto Papa
Department of Science and Technology
Parthenope University of Naples
Naples, Italy
umberto.papa@uniparthenope.it

Salvatore Ponte
Department of Engineering
University of Campania "L. Vanvitelli"
Aversa (CE), Italy
salvatore.ponte@unicampania.it

Giuseppe Del Core
Department of Science and Technology
Parthenope University of Naples
Naples, Italy
giuseppe.delcore@uniparthenope.it

***Abstract*—Unmanned Aircraft Systems (UAS) have gained impetus in the last decade from increasing civil, scientific, military, commercial and recreational applications (e.g. urban traffic monitoring, war zone defense and monitoring, archaeological site prospection, inspection of electrical power lines, etc.). Autonomous flight, management and control of Unmanned Aerial Vehicles (UAVs) are important issues in many professional and research applications. This paper focuses on trajectory measurement and control using two sensors (Angle of Attack, AOA and Angle of Sideslip, AOS) for speed and attitude estimation. The sensors involved in the analysis are a pressure (static and dynamic) sensor and an Inertial Measurement Unit (IMU). Kalman Filtering (KF) has been applied for measurement noise removal and data fusion. The theoretical analysis of the KF shows that global exponential stability of the estimation error is achieved under these conditions. The method has been tested using experimental data from a small quadrotor, with a legacy autopilot to provide basic estimates of UAV velocity and attitude and comparing them with the sensors data. AOA and AOS have been validated via correlation between the AOA estimate and vertical accelerometer measurements, since lift force can be modeled as a linear function of AOA in normal flight. Results from several flight tests confirm the validity of the approach to trajectory determination.**

Keywords—Unmanned Aircraft Systems, IMU, Pressure Sensors, Autonomous Flight, Flight Mechanics, Sensor Fusion, Kalman Filtering.

I. INTRODUCTION

Unmanned Aerial Vehicles (UAV) are an easy-to-use and economical way for a large number of tasks that can be fulfilled without human involvement. UAVs can also be an optimal solution as a test bench for new sensors systems or embedded flight management systems. When subsystems are integrated to improve characteristics such as estimation of the vehicle's state vector, autonomy and GNC (Guidance, Navigation and Control), we talk about Unmanned Aircraft Systems (UAS), categorized as semi-autonomous, remotely operated and fully autonomous [1].

Typically, for real-time trajectory and speed estimation, IMUs (Inertial Measurement Unit) are used. Much work has been published in the field of extrapolation, filtering and fusion of IMU and other sensor data (GPS, LIDAR, Sonar, etc.) for attitude and velocity estimation [2-6] and for meteorology and wind estimation. Usually, large airplanes are equipped with probes, properly calibrated along the fuselage, that measure wind velocity, Angle of Attack (α) and Sideslip Angle (β), variables that contain useful information about performance and safety in normal and abnormal flight conditions.

However, few papers consider practical methods for AOA and AOS estimation on UAVs or light aircrafts, because of large weight, size, cost and power consumption. Yet, estimates of these parameters can be used for fault detection and changes due to structural damage or adverse flight condition that could alter the aerodynamic coefficients of an UAV, and could also allow precise control of small UAVs in particular maneuvers, such as vertical landing [7]. A comprehensive review of some methodologies and estimation approaches for typical fixed-wing and rotary-wing UAVs can be found in [8].

The advent of miniaturization has permitted the use of small, low-weight, low-power sensors, allowing the possibility of installing a Pitot tube on a UAV. The Pitot system devised in this work is composed by dynamic and static pressure sensors, both managed by a microcontroller Arduino. The paper describes a micro Pitot tube installed on a small quadrotor for AOA and AOS estimation from wind velocity measurements. Kalman-filter based data fusion techniques use the Pitot-derived estimates and accelerometric data from an IMU, to provide an estimate of UAV attitude [9, 10]. Experimental data have been collected out during several flight tests (indoor and outdoor) conducted by the PFDL (Parthenope Flight Dynamic Laboratory) team of the University of Naples "Parthenope" (Italy). Indoor sessions were needed for system setup and calibration.

The paper is structured as follows: after establishing the theoretical framework (kinematic model and Kalman-filter-based estimation technique), the sensors used are characterized and the attitude estimation methodology is presented. Successively, flight tests and analysis of test results are described. Final considerations and future work directions conclude the paper.

II. Theoretical Framework

We start from the aircraft kinematics [11], referencing to Figure 1. Let $\boldsymbol{v_{ac}^B} = (u, v, w)^T$ denote the velocity vector (relative to Earth) in the aircraft's body coordinate frame (CF), with T denoting transposition. Let $\boldsymbol{v_{ac}^N} = (u_g, v_g, w_g)^T$ denote the vector containing its components referred to an Earth-Fixed North-East-Down (NED) CF. The UAV kinematics are:

$$\begin{aligned} \dot{u} - rv + qw &= a_x \\ \dot{v} - pw + ru &= a_y \\ \dot{w} - qu - pv &= a_z \end{aligned} \tag{1}$$

where $\boldsymbol{a} = (a_x, a_y, a_z)^T$ is the acceleration, and p, q, r are the angular rates.

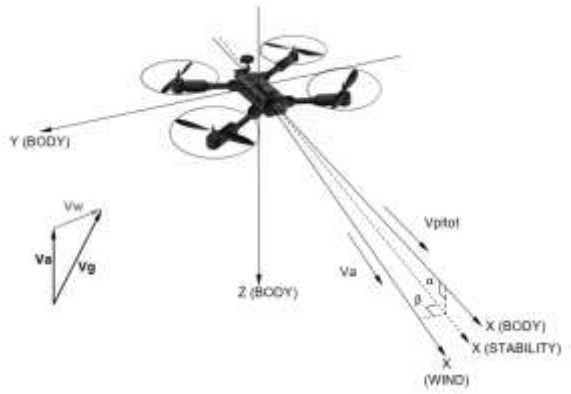

Figure 1. *Airspeed definition and wind triangle.*

The wind velocity vector relative to the Earth, in the NED CF, is $\boldsymbol{v_w^N} = (u_w, v_w, w_w)^T$.

The aircraft velocity $\boldsymbol{v_r}$ relative to the wind velocity is:

$$\boldsymbol{v_r} = \boldsymbol{v_g} - \boldsymbol{v_w} \tag{2}$$

The rotation matrix for moving from the NED frame to the body frame, R_N^b, is defined by roll (ϕ), pitch (θ) and yaw (ψ) angles. Therefore, the relative velocity $\boldsymbol{v_r}$ in the body CF is:

$$\begin{pmatrix} u_r \\ v_r \\ w_r \end{pmatrix} = \begin{pmatrix} u \\ v \\ w \end{pmatrix} - R_N^b \begin{pmatrix} u_w \\ v_w \\ w_w \end{pmatrix} \tag{3}$$

The AOA, α and AOS, β, are the angles between $\boldsymbol{v_r}$ and the body CF: α, β and the airspeed V_a are given by:

$$\alpha = \tan^{-1}(w_r/u_r) \tag{4}$$

$$\beta = \tan^{-1}(v_r/V_a) \tag{5}$$

$$V_a = \sqrt{u_r^2 + v_r^2 + w_r^2} \tag{6}$$

Assuming low wind velocities, AOA corresponds to pitch angle, and the AOS coincides with the yaw angle. The roll angle can be estimated by using accelerometers as tilt sensors, or integrating the rate gyro measurements from an onboard IMU. Finally, he Pitot velocity v_{pitot} is derived from Bernoulli's equation:

$$v_{pitot} = \sqrt{K\,\frac{2\Delta P}{\rho}} \tag{7}$$

where ΔP is the dynamic pressure, ρ is the air density and K is a correction factor. Using (4), (5) and (6), the Pitot velocity can also be expressed as:

$$V_{pitot}^2 = |V_a|^2 \cos\alpha \cos\beta \tag{8}$$

Combining (7) and (8) we obtain:

$$V_a^2 = \frac{V_{pitot}^2}{\cos\alpha\cos\beta} = \frac{\Delta P}{\rho\cos\alpha\cos\beta/(2K)} = \frac{\Delta P}{KA} \tag{9}$$

Before takeoff, any bias affecting the dynamic pressure has to be removed, if present. The scaling factor KA can be used between the dynamic pressure and the squared Pitot speed, when AOA and AOS are small.

The Kalman filtering algorithm applied for data fusion and measurement noise estimation and removal is the well-known predictor-corrector sequence synthetically described in Table 1 [12].

Table 1*. Kalman Filter Algorithm.*

Initialization (provided by the user)	$\hat{x} = x_0$ $P = P_0$
Time update (predictor)	$\hat{x}_{k\|k-1} = F_k\hat{x}_{k-1\|k-1}$ $P_{k\|k-1} = F_kP_{k-1\|k-1}F_k^T + Q_k$
Measurement update (corrector)	$\tilde{y}_k = z_k - H_k\hat{x}_{k\|k-1}$ $S_k = H_kP_{k\|k-1}H_k^T + R_k$ $K_k = P_{k\|k-1}H_k^TS_k^{-1}$ $\hat{x}_{k\|k} = \hat{x}_{k\|k-1} + K_k\tilde{y}_k$ $P_{k\|k} = (I - K_kH_k)P_{k\|k-1}$

where $\hat{x}_{k|k-1}$ is the predicted *a priori* state estimate (before including observation information at the current timestep), F is the state transition model, $P_{k|k-1}$ is the predicted *a priori* estimate covariance matrix, Q_k is the covariance matrix of the process noise, $\tilde{y}_k$ is the innovation, H_k is the measurement matrix, $z_k = H_kx_k + \nu_k$ is the current measurement (data), R_k is the covariance matrix of the observation noise ν_k (assumed zero-mean Gaussian white), K_k is the optimal Kalman gain, $\hat{x}_{k|k}$ is the updated *a posteriori* state estimate, and $P_{k|k}$ is the updated *a posteriori* estimate covariance matrix.

III. Sensors System

The system used for velocity and attitude estimation is composed by:

- Differential pressure sensor, MPX2010DP;
- Static pressure sensor, BMP180;
- IMU, 10DOF;
- Microcontroller Arduino Mega 2560.

A. MPX2010DP

As stated in Eq. (7), the dynamic pressure is necessary for velocity estimation. The MPX2010 (**Figure 2**) series silicon piezo resistive pressure sensor [13] provides a very accurate and linear voltage output directly proportional to the applied pressure. In this case, the DP (differential pressure) sensor is chosen. Sensor parameters are described in Table 2.

***Figure 2**. Differential pressure sensor MPX2010DP.*

These sensors house a single monolithic silicon die with the strain gauge and thin film resistor network integrated. The sensor is laser-trimmed for precise span, offset calibration and temperature compensation, allowing optimal linearity, little temperature hysteresis and excellent response time.

***Table 2**. MPX2010DP operating characteristics.*

Pressure Range: from 0 to 10 kPa (0 to 1.45 psi)
Supply Voltage and Current: 10 Vdc, 6.0 mAdc
Temperature compensated over 0° to +85° C
Operating Temperature: –40 to 125 °C
Full scale span: 25 mV
Sensitivity: 2.5 mV/kPa
Response Time: 1 ms

B. BMP180

In order to have redundant static pressure measurements, the digital pressure sensor BMP180 (Figure 3) has been enclosed in the system. The BMP180, produced by Bosch Sensortec, consists of a piezoresistive sensor, an analog-to-digital converter, a control unit with E^2PROM and a serial I^2C interface, that allows for easy system integration by direct connection to commercial microcontrollers [14]. Pressure data, in the range 300-1100 hPa (from +9000 m to -500 m related to sea level) and temperature data are compensated by the calibration data of the embedded E^2PROM.

***Figure 3**. Barometric sensor, BMP180.*

C. 10-DOF IMU and accelerometer calibration

The 10-DOF IMU sensor [15], built by DFRobot, is a compact-size (26x18mm) board, fully compatible with the Arduino microcontroller family, and integrates the Analog Device's ADXL345 accelerometer [16], Honeywell's HMC5883L magnetometer [17], the ITG-3205 gyro [18] and the Bosch BMP280 barometric pressure sensor. The sensor, shown in Figure 4, is a polysilicon surface micro-machined structure built on top of a silicon wafer. Polysilicon springs suspend the structure over the surface of the wafer and provide a resistance against acceleration forces.

***Figure 4**. 10-DOF Mems IMU.*

D. Microcontroller Arduino

The Arduino Mega 2560 (Figure 5) board is a microcontroller board based on the ATmega2560. It has 54 digital input/output pins (of which 14 can be used as PWM outputs), 16 analog inputs, 4 UARTs (hardware serial ports), a 16-MHz crystal oscillator, a USB connection, a power jack, an ICSP header, and a reset button. It contains everything needed to support the microcontroller; simply connecting it to a computer with a USB cable or powering it with an AC to DC adapter or battery allows the board to get started and work in an integrated development environment (IDE) based on the Processing language project [19]. In our experimental session, the microcontroller power supply comes from the small quadrotor.

***Figure 5**. Arduino Mega 2560.*

IV. Simulations and Results

The outdoor simulation campaigns have been done considering the system (Fig. 6) installed on the small quadrotor. Previously, an indoor experimental campaign was performed in the Parthenope Flight Dynamic Lab (PFDL), University of Naples "Parthenope", Naples, Italy.

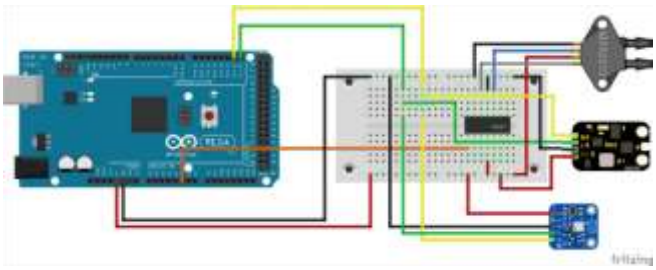

***Figure 6**. Electric Scheme of the system developed.*

Due to SARS-CoV-2 emergency, the planned outdoor simulations and data collecting campaigns have not been performed. Indoor simulations allowed us to consider only the velocity estimation from the micro Pitot tube. No attitude evaluations have been done. The system shown in Figure 6 was tested using a fan as airflow generator, and acquiring the differential pressures from the MPX2010DP sensor. The 10-bit sensor's measurement range is 0-1023. Figure 7 shows a sample of raw pressure data collected during a 100-s, 1-Hz acquisition.

To reduce measurement noise, simple low-pass filtering has been applied to the raw data, post-processed in the Matlab® software environment: the result is shown in Figure 8. Preliminarily, for calibration purposes, i.e. sensor bias estimation, digital pressure data (10-bit strings) have been collected in quiet airflow ($v_w = 0$).

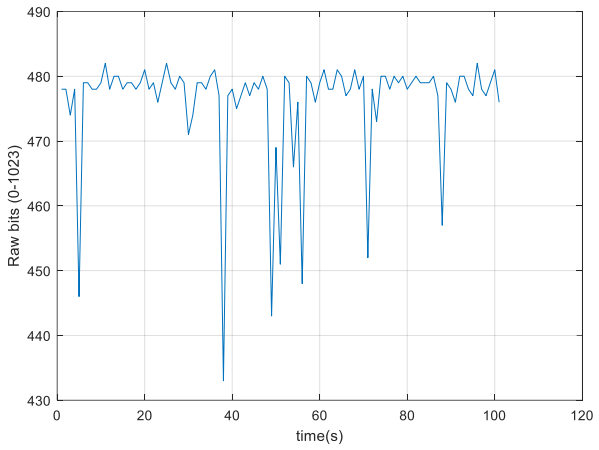

Figure 7. Raw pressure data from MPX2010DP. v_w=0.

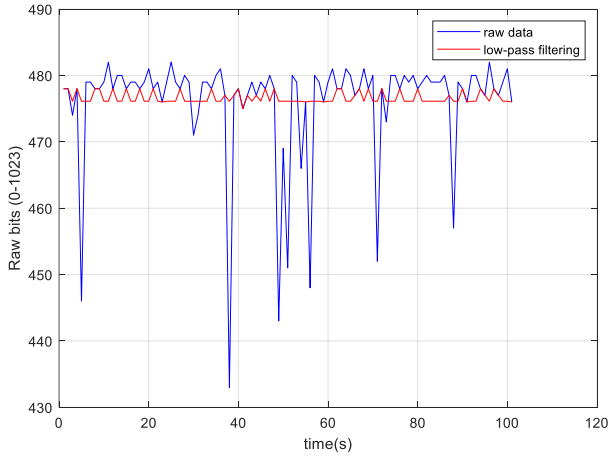

Figure 8. Low-pass filtered and Raw data from MPX2010DP. V=0.

With $v_w = 0$, the sensor's DN (digital number) output is 512, which corresponds, according to the following relation, to 2.5V:

$$Voltage = \left(\frac{5}{1023}\right) * DN \tag{10}$$

As shown in Figure 9, the average voltage acquired at $v_w = 0$ is about 2.33V. This bias that must be applied to measurements with different values of v_w, to estimate the pressure and velocity as in Eq. (7).

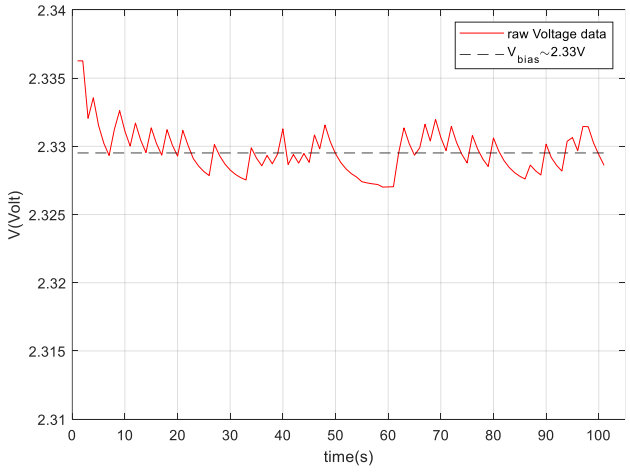

Figure 9. Bias voltage @ $v_w = 0$.

As previously said, the experiments have been performed indoor, mounting the equipment on a test bench. The environmental conditions were: 40% relative humidity at 20 °C. Data have been collected at a sample rate of 1Hz. After bias estimation and sensor calibration, a session has been done considering two monitoring points, with $v_w = 20$ and 40 km/h respectively.

The airflow velocity is checked with a digital anemometer (Proster Handheld Anemometer PST-TL017 [20]), shown in Figure 10.

Figure 10. PST-TL017 - Anemometer used for airflow speed check.

The acquired raw signal is shown in Figure 11.

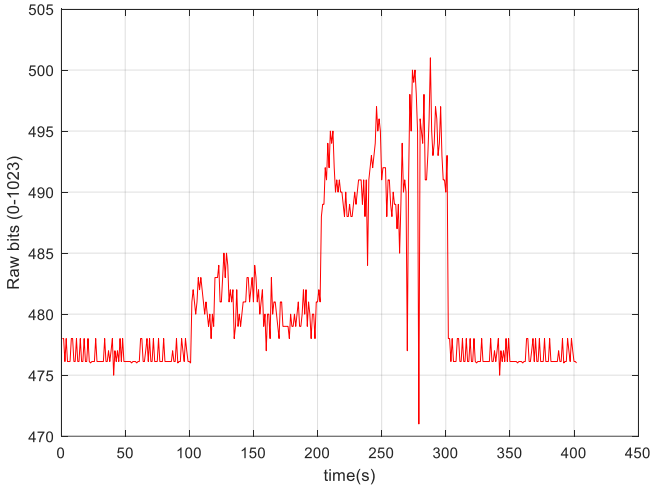

Figure 11. Raw data collection (DN of sensor measurement).

Figure 12 shows the final velocity acquisition (raw data vs. Kalman filtered data), compared with the reference speed, acquired by the digital anemometer.

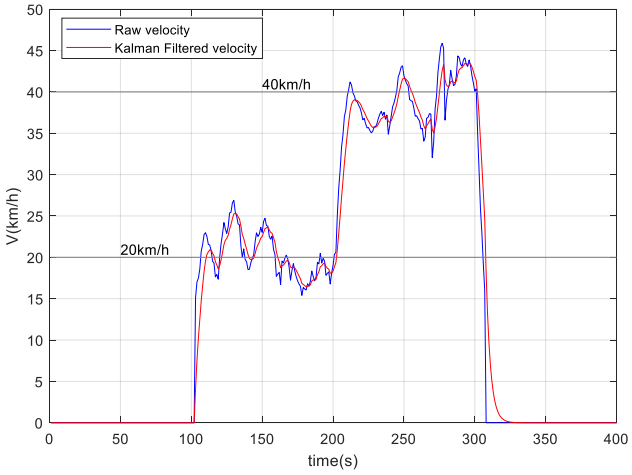

Figure 12. Velocity. Raw vs. Kalman Filtered.

Furthermore, temperature, humidity (measured by the sensor DHT11) and altitude (static pressure, acquired by the BMP180 sensor) have been acquired, in order to have some redundancies and implement multisensor fusion strategies. The data trend during the acquisition campaign is shown in Figure 13.

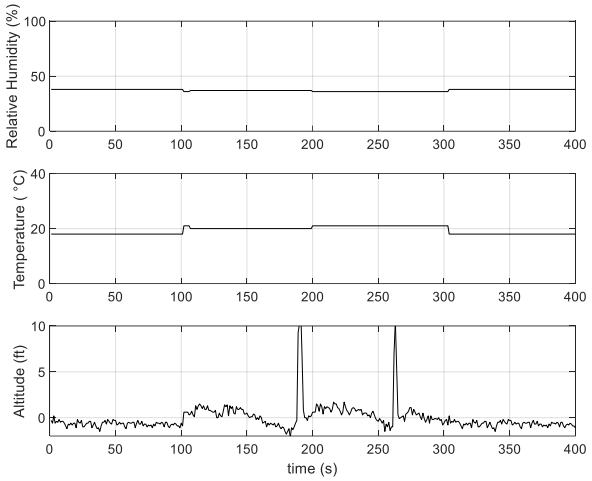

***Figure 13**. Temperature, humidity and altitude data acquired during experimental campaigns.*

V. Conclusion and Further Work

This paper presented the mathematical modeling (kinematic relationships) and the first experimental steps for small UAV velocity estimation using a differential pressure sensor like an aircraft Pitot tube. Preliminary results show the feasibility of the approach, and the possibility of designing control laws for increasing the flight envelope by means of estimation of AOA. Due to logistics problems (SARS-CoV-2 emergency), it was not possible to make outdoor experiments and UAS attitude evaluation in different wind conditions (steady and turbulent winds) and flight scenarios (climb, hover, curved paths, descents, loops). Currently, this paper presents preliminary experimental data for wind velocity estimation and pressure measurements with the MEMS sensor suite previously described.

Further steps will obviously concentrate on producing data with a prototype of the system mounted on the UAS, and exploring the correlation between AOA and AOS estimates and UAS attitude angles in both normal and heavy wind conditions. Future work will focus on validation of the methodologies devised for attitude estimation via AOA and AOS measurements, since attitude information data are important for UAS monitoring and control during special tasks and unconventional missions, or for particular UAS structural design, such as the hybrid UAV proposed in [21].

References

[1] Papa, U., *Embedded Platforms for UAS Landing Path and Obstacle Detection*. Studies in Systems, Decision and Control, vol 136. Springer, Cham, 2018.

[2] Abdelkrim, N. and Aouf., N. "Robust INS/GPS sensor fusion for UAV localization using SDRE nonlinear filtering." *IEEE Sensors Journal* 10.4 (2010): 789-798.

[3] Gross, J. N., Gu, Y., Rhudy, M. B., Gururajan, S., and Napolitano, M. R. (2012). Flight-test evaluation of sensor fusion algorithms for attitude estimation. *IEEE Transactions on Aerospace and Electronic Systems*, *48*(3), 2128-2139.

[4] Yang, X., Mejias, L., and Garratt, M. (2011). Multi-sensor data fusion for UAV navigation during landing operations. In *Proceedings of the 2011 Australian Conference on Robotics and Automation* (pp. 1-10). Australian Robotics and Automation Association Inc., Monash University.

[5] Del Pizzo, S., Papa, U., Gaglione, S., Troisi, S., and Del Core, G. (2018). A Vision-based navigation system for landing procedure. *Acta IMEKO*, *7*(2).

[6] Ariante, G., Papa, U., Ponte, S., and Del Core, G. (2019). UAS for positioning and field mapping using LIDAR and IMU sensors data: Kalman filtering and integration. In *2019 IEEE International Workshop on Metrology for AeroSpace*, June 19-21, 2019, Torino, Italy.

[7] Johansen, T. A., Cristofaro, A., Sørensen, K., Hansen, J. M., Fossen, T. I. (2015). On estimation of wind velocity, angle-of-attack and sideslip angle of small UAVs using standard sensors. Proc. *2015 International Conference on Unmanned Aircraft Systems (ICUAS),* Denver Marriott Tech Center, Denver, CO, USA, June 9-12, 2015, pagg. 510-519.

[8] Sankaralingam, L., Ramprasadh, C. (2020). A comprehensive survey on the methods of angle of attack measurement and estimation in UAVs. *Chinese Journal of Aeronautics*, Vol. 22, Issue 3, March 2020, pp. 749-770. DOI: https://doi.org/10.1016/j.cja.2019.11.003.

[9] De Marina, H. G., Pereda, F. J., Giron-Sierra, J. M., and Espinosa, F. (2011). UAV attitude estimation using unscented Kalman filter and TRIAD. *IEEE Transactions on Industrial Electronics*, *59*(11), 4465-4474.

[10] Ariante, G., Papa, U., Ponte, S., & Del Core, G. (2019). UAS for positioning and field mapping using LIDAR and IMU sensors data: Kalman filtering and integration. In *2019 IEEE 5th International Workshop on Metrology for AeroSpace (MetroAeroSpace)* (pp. 522-527). IEEE.

[11] Beard, R. W., and McLain, T. W. (2012). *Small unmanned aircraft: Theory and practice*. Princeton University Press.

[12] Grewal, M. S., Andrews, A. P. (2008). *Kalman Filtering – Theory and Practice Using MATLAB®*, 3rd Edition. John Wiley & Sons, Inc.

[13] NXP (2008). *MPX2010 sensors Datasheet. Rev. 13*.

[14] Bosch Sensortec (2015). *BMP180 Digital pressure sensor*, Rev. 2.8, Doc. No. BST-BMP180_DS000-12.

[15] DFRobot (2018). "10-Dof MEMS IMU Sensor V2.0", https://www.dfrobot.com/wiki/index.php/10_DOF_Mems_IMU_Sensor_V2.0_SKU:_SEN0140. Accessed March 2020.

[16] Analog Devices (2009). Small, Low Power, 3-Axis ±3g Accelerometer ADXL335-345. Rev. 0. One Technology Way, Norwood, MA, USA. https://www.sparkfun.com/datasheets/Components/SMD/adxl335.pdf Accessed March 2020.

[17] Honeywell (2013). 3-Axis Digital Compass IC HMC5883L. https://aerocontent.honeywell.com/aero/common/documents/myaerospacecatalogdocuments/Defense_Brochuresdocuments/HMC5883L_3-Axis_Digital_Compass_IC.pdf . Honeywell, Plymouth, Mn, USA. Accessed March 2020.

[18] InvenSense Inc. (2010). ITG-3200 Product Specification – Revision 1.4 https://www.sparkfun.com/datasheets/Sensors/Gyro/PS-ITG3200-00-01.4.pdf . Accessed March 2020.

[19] Arduino (2020). Arduino Software (IDE) download page, https://www.arduino.cc/en/main/software. Accessed March 2020.

[20] Proster® (2012). Proster TL017 Handheld Anemometer Wind Speed Meter Scale Gauge. Available online: http://www.prostereu.com/index.php/2015/07/24/tl017/. Accessed March 2020

[21] Papa, U., Ponte, S., & Del Core, G. (2017). Conceptual design of a small hybrid unmanned aircraft system. *Journal of Advanced Transportation*, 2017(1): 1-10.